NANO LETTERS

2007
Vol. 7, No. 12
3884−3890

Sizing up the Exciton in Complex-Shaped Semiconductor Nanocrystals

Jeongho Kim, P. Sreekumari Nair, Cathy Y. Wong, and Gregory D. Scholes*

Department of Chemistry, 80 St. George Street, Institute for Optical Sciences, and Center for Quantum Information and Quantum Control, University of Toronto, Toronto, Ontario, M5S 3H6 Canada

Received August 26, 2007; Revised Manuscript Received October 16, 2007

ABSTRACT

We report a spectroscopic study of how nanocrystal shape influences exciton size. The effective exciton size in complex-shaped nanocrystals is examined by comparing exciton fine structure relaxation rates, measured by the ultrafast polarization transient grating method, to an extensive empirical calibration curve that relates the relaxation rates of quantum dots and nanorods to their diameters. It is found that the overall nanocrystal shape is important for determining the effective exciton size in nanocrystals. How nanocrystal shape plays a role in quantum confinement and therefore exciton shape is qualitatively discussed based on these experimental results.

Over the past decade, colloidal semiconductor nanocrystals (NCs) have attracted considerable interest owing to their size-dependent optical and electronic properties[1−6] and their potential for applications in optoelectronic nanodevices.[7−12] For example, photoexcited NCs can have a high photoluminescence quantum yield and narrow bandwidth, and the emission peak can be tuned in color by simply changing the NC size. Accordingly, a lot of studies have been made toward revealing the size-dependent photophysics and electronic structure of NCs. Recent advances in chemical synthesis have enabled the discovery of sophisticated shape control protocols for colloidal NC growth. As a result, NCs with increased degrees of structural complexity have been synthesized, for example, NCs with rod, teardrop, pyramid, bullet, and tetrapod shapes as well as hyperbranched dendritic NCs.[13−21] Studies of NC shape control have been given further impetus by potential technological benefits. For example, NC-polymer hybrid solar cells employing nanorods instead of (spherical) quantum dots (QDs) demonstrated improved solar conversion efficiency owing to enhanced electron transport efficiency through the NC phase.[9] Therefore, it is of fundamental interest to discover the implications of shape on optical and electronic properties of NCs.

With the ability to control NC shape, a focus of NC research is shifting toward investigating the shape-dependent properties of NCs. In NCs smaller in all dimensions than the exciton Bohr radius, the three-dimensional (3D) quantum confinement regime, the size of the exciton is dictated by the physical dimensions of the NC rather than by the strength of the electron−hole Coulombic interaction. Then, the properties of NC excitons can be sensitive to the NC shape, and a fundamental and important question arises: What are the implications of NC shape on photophysics of the NCs? To answer this question, there have been several studies of how NC shape affects the electronic properties of NCs.[22−26] Whereas the variation of NC size mainly changes energy level spacing (i.e., band gap), the change in shape might cause more subtle changes in electronic structure of excited states, for example, modification of the fine structure, overall shape and symmetry of wavefunctions, polarization, and localization of electronic states.[25,27−30] Thus, shape control of NCs provides a means of fine-tuning the electronic properties of NCs.

At present our understanding is limited to variations of the band gap (and optical gap). For example, the band gap variation with respect to size and shape of nanorods was studied by photoluminescence measurements of CdSe[23] and InAs[16] nanorods with various diameters and aspect ratios. It was shown that the band gap of nanorods decreases with increasing aspect ratio toward the value expected of true 1D quantum wires with different degrees of correlation with length for CdSe and InAs nanorods. These experimental trends were later captured by $k\cdot p$ calculations for CdSe nanorods.[24] Recently, using scanning tunneling microscopy, Banin and co-workers have successfully detected individual valence and conduction electronic states in InAs NCs and indirectly identified their *s*- and *p*-symmetry features.[31] But, we are still far from detecting the shape-induced change in

* To whom correspondence should be addressed. E-mail: gscholes@chem.utoronto.ca.

10.1021/nl072149f CCC: $37.00
Published on Web 11/03/2007

electronic states of NCs. The search for a deeper understanding of the implications of nanoscale shape on the properties of nanoscale excitons[32] calls for a novel spectroscopic approach.

The challenge in spectroscopic studies of NC shape effects lies in that it is extremely difficult experimentally to detect subtle changes in the electronic states induced by NC shape change. Sensitive spectroscopic studies are particularly limited by sample polydispersity and the resultant inhomogeneous line broadening.[33] This limitation explains the relative lack of experimental studies on NC shape effects compared to theoretical work. In an effort to circumvent this limitation, there have been single-particle studies of the optical properties of nanorods[34−36] and nanowires,[37,38] revealing the details of the electronic structure in these 1D semiconductor nanostructures. However, only limited information could be obtained from such studies due to difficulty in implementation of the experiments. In the present communication, we report a spectroscopic study of the NC shape effect on the size and shape of NC excitons. We demonstrate on the basis of experimental measurements that the detailed shape of NCs is important for determining the effective size, as well as shape, of excitons confined in CdSe NCs. We propose that the exciton in complex-shaped Wurtzite NCs is spread out predominantly over the larger physical dimensions transverse to the *c*-axis, which is in good agreement with theoretical predictions.[25,27−29] As a measure of exciton delocalization in NCs, we have extended our recent ultrafast measurements of CdSe NC fine structure relaxation using the cross-polarized heterodyned third-order transient grating (CPH-3TG) technique. Careful studies of quantum dots and nanorods establish a calibration curve according to the empirical observation that the dominant relaxation rate constant scales inversely as the fourth power of the exciton diameter. Comparing measurements of NCs with more complex shape to this calibration curve suggests the effective diameter of the exciton in each case, which we compare to the physical shape of the NC as measured by TEM.

The CPH-3TG technique has been demonstrated to be an effective method of measuring population transfer dynamics in the exciton fine structure of NCs as well as estimating very small interactions between the exciton fine structure states.[39,40] The population transfer dynamics measured by this technique accompanies spin flip transitions whereby the total angular momentum of an exciton changes its sign by population transfer among the $F = +1$ and $F = -1$ exciton fine structure states. The method measures such transitions between states with degenerate energy levels, provided the sign of the total angular momentum of the exciton changes. This is unlike "normal" ultrafast techniques that monitor energy relaxation.

Our recent studies of a variety of nanorods with different sizes and shapes over an extensive time range of up to hundreds of picoseconds suggest that the origin and mechanism of the transitions in the exciton fine structure are much more complicated[41] than the single-step direct transfer process between $F = \pm 1$ exciton states that we initially proposed.[40] To account for that, we will term the dynamics probed by this CPH-3TG technique as the exciton fine structure relaxation (EFSR) in a broader sense, rather than exciton spin relaxation that was used in our previous papers.[39,40,42] In this paper, we will not discuss the origin and mechanism of the transitions in the exciton fine structure, which is still under investigation in our group. However, it was clearly verified that the size dependence of the dominant relaxation rate between $F = +1$ (-1) and $F = -2$ $(+2)$ states in the CdSe QDs and nanorods shows a distinctive scaling law of $1/d^4$, where d is the diameter of a plane perpendicular to the *c*-axis. Although theoretical justification for the relationship is still underway, this empirical relationship for the principal EFSR rate determined from careful studies of quantum dots and nanorods can serve as a calibration curve for determining the effective exciton size in complex-shaped NCs as long as the EFSR rate is measured and analyzed in a consistent manner among the sample under investigation.

NCs of various shapes were synthesized by a thermolysis reaction of a dual precursor system using a multiple-injection strategy.[21] The shape control was achieved by carrying out multiple reagent injections and varying the type of surfactant introduced during the growth of the NCs. Figure 1 shows the representative transmission electron microscopy (TEM) images of samples used for measurements in this work. The corresponding absorption spectra of each sample can be found in ref 21. All the complex-shaped NCs were derived from rod-shaped seed nanocrystals by changing the relative concentration of surface ligands and shape-directing reagent as well as NC growth time. The bullet, Figure 1b, has a similar shape to the rod except that one end is elongated and narrowed along the *c*-axis. The trigonal pyramid, Figure 1d, evolves from the bullet with subsequent injections of ligands and shape-directing reagent, by which the tip of the rod is elongated and three (100)-type faces of the hexagonal prism are eliminated during growth. The sample, Figure 1c, can be considered as the intermediate stage between bullet, Figure 1b, and trigonal pyramid, Figure 1d, although its shape is closer to trigonal pyramid. The multipod, Figure 1e, is formed with arms growing in the [101] direction, forming a tripod or tetrapod shape. The multipod pyramid, Figure 1f, is of pyramidal shape, but with a multigonal base plane and small arms bulging from the base, and it results from growth of arms along both [001] and $[00\bar{1}]$ axes.

The physical shape parameters of the NCs were determined from TEM images, and are listed in Table 1. The size distribution of the samples is typically 10−15% standard deviation both in diameter and length. It should be noted that the size parameters shown in Table 1 are the largest sizes in each dimension. In each case of complex-shaped NCs, the size in each dimension gradually varies along each axis, so the size cannot be defined unambiguously by a certain single value. Therefore, we determined the upper limit in each dimension, for example, the base diameter, d_{base}, corresponds to the diameter of the largest base plane in a complex-shaped NC, as seen in the TEM projections in Figure 1, and not that of a narrower region.

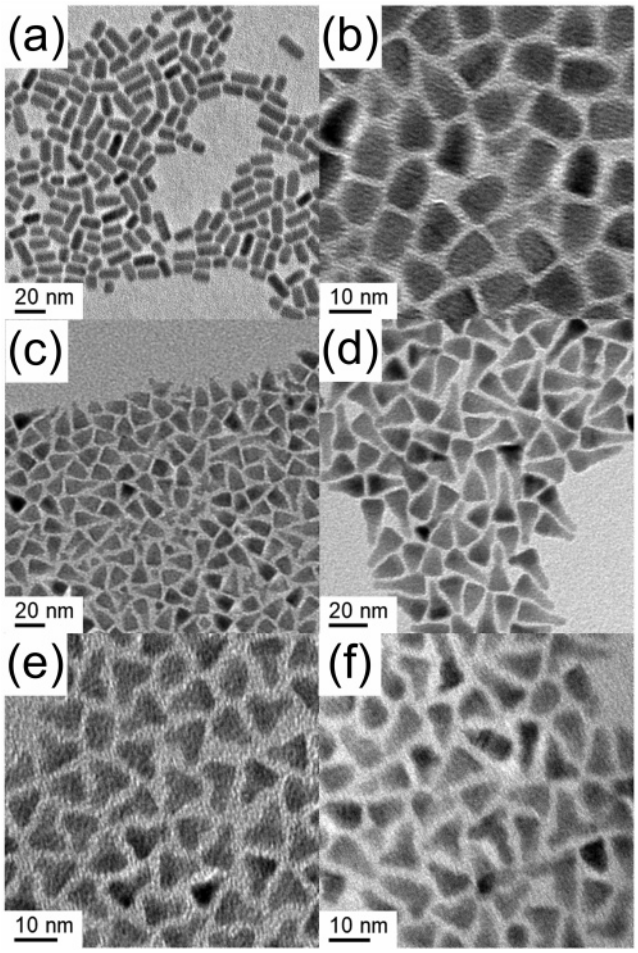

Figure 1. Representative TEM images of various shapes of NCs used in the 3-TG measurements. (a) R1 (rod), (b) B1 (bullet), (c) TP1 (trigonal pyramid), (d) TP2 (trigonal pyramid), (e) M1 (multipod), and (f) MP2 (multipod pyramid). The detailed shape parameters of the samples are listed in Table 1. The scale bar is 10 or 20 nm for each of the TEM images.

Heterodyned 3-TG signals were measured by an experimental setup using a diffractive optic. The details of the setup have been described elsewhere.[40] Each sample, a dilute solution of CdSe NCs in toluene, was photoexcited in resonance with the lowest exciton absorption band by ultrashort laser pulses at a 1 kHz repetition rate. The laser center wavelength was tuned to be 5−7 nm to the red from the lowest exciton band to ensure that a relatively narrow size distribution of nanorods are resonantly excited, as determined by the laser spectrum (~30 nm full width at half-maximum) at each excitation wavelength. Depending on the center wavelength of laser spectrum, pulse durations of 30−35 fs were obtained from 3-TG autocorrelation measurements using carbon tetrachloride at the sample position. To prevent any sample degradation, biexciton formation, or thermal grating contributions to the signal, the pulse energy was kept at less than 5 nJ/pulse. The intensities of both pump and probe beams were attenuated until the early time signal shape did not change. To ensure that the sample had not photodegraded during the measurements, the absorption spectrum of the sample was collected before and after each measurement. All of the measurements reported in the present work were performed at room temperature.

The CPH-3TG technique is based on the theoretical finding that excitons of conserved and flipped spins among the $F = \pm 1$ exciton states radiate third-order signals of opposite signs in a randomly oriented ensemble of quantum dots. In other words, the heterodyned cross-polarized 3-TG signals of CdSe quantum dots can be written as

$$I_{\mathrm{HET}}(t_p) \propto \int_0^{\infty} dt\, \mathrm{Re}\{E^*_{\mathrm{LO}}(t_p, \Delta\phi)\cdot P^{(3)}(0, t_p, t) \times [C(n_C^{+1} + n_C^{-1}) + C'(n_F^{+1} + n_F^{-1})]\} \quad (1)$$

where $E^*_{\mathrm{LO}}(t_p, \Delta\phi)$ is the electric field of the local oscillator, $P^{(3)}(0, t_p, t)$ is the induced third-order polarization, and $n_C^{+1}(n_C^{-1})$ and $n_F^{+1}(n_F^{-1})$ are the populations of conserved and flipped excitons probed in the $F = +1$ (-1) states, respectively. The coefficients, C and C', are rotational averaging factors and have values of 2/15 $(-2/15)$ and $-2/15$ (2/15) for the 3-TG signals using cross-linear polarization sequence of VHVH (VHHV), respectively. Thus, by measuring the cross-polarized 3-TG signals, we can keep track of the time evolution of conserved or flipped populations between the $F = \pm 1$ exciton states.[39]

The imaginary (absorptive) part of 3-TG signals of NCs of various shapes and sizes were measured with different polarization sequences, VVVV, VHVH, and VHHV, and data are shown in Figure 2. The VVVV signal shows a slow decay reaching over a nanosecond time scale and reflects the dynamics of exciton recombination. In contrast, the cross-polarized signals with VHVH and VHHV polarization sequences decay much faster predominantly in several to tens of picoseconds. It is notable that initial decays of VHVH and VHHV signals have opposite signs, which directly indicate dynamics of EFSR represented in each cross-polarized signal.[39] The cross-polarized signals were fit by three-exponentials

$$I_{\mathrm{VHVH}}(t_p) = [A_1 \exp(-k_{s1}t_p) + A_2 \exp(-k_{s2}t_p) + A_3] I_{\mathrm{VVVV}}(t_p) \quad (2)$$

where k_{s1} and k_{s2} are the EFSR decay rates of fast and slow decay components, respectively, and $I_{\mathrm{VVVV}}(t_p)$ is the decay profile of the VVVV 3-TG signal as a function of the pump−probe time delay, t_p, and A_3 is the amplitude of the slow exciton recombination dynamics represented by the VVVV signal. In our previous work,[40] double exponential EFSR decay dynamics was observed in the CPH-3TG signals of CdSe nanorods with large diameters. Among the double exponential decay components, the rate of the fast EFSR component (k_{s1}) is attributed to a transition rate between $F = +1$ (-1) and $F = -2$ $(+2)$ states in the exciton fine structure of CdSe NCs and shows a strong correlation with respect to the diameter of the NCs by a scaling law of $1/d^4$. Thus, here we use this fast EFSR rate determined from the above fitting procedure as a way of gauging the exciton size in complex-shaped NCs.

Table 1. Shape Parameters, EFSR Rates, and Effective Exciton Sizes of Nanorods and Complex-Shaped NCs

label	shape	diameter, d_{base} (nm)[a]	length (nm)[a]	Aspect ratio[a]	k_{s1}^{VHVH} (ps^{-1})[b]	k_{s1}^{VHHV} (ps^{-1})[b]	d_{fit} (nm)	Δd ($\Delta d/d_{fit}$)[c]	d_{sph} (d_{sph}/d_{fit})
R1	rod	6.29 (0.67)	10.22 (1.06)	1.63 (0.19)	0.223	0.221	7.33	−1.04 (−0.142)	
R3	rod	8.41 (0.81)	17.63 (2.51)	2.11 (0.32)	0.092	0.104	9.29	−0.88 (−0.094)	
R2	rod	7.31 (0.78)	10.38 (0.80)	1.43 (0.14)	0.198	0.190	7.57	−0.26 (−0.035)	
B1	bullet	8.90 (0.51)	12.73 (0.91)	1.44 (0.13)	0.108	0.105	8.90	0.00 (0.000)	
B2	bullet	9.92 (0.78)	16.79 (1.32)	1.70 (0.19)	0.076	0.100	9.76	0.16 (0.016)	
R5	rod	10.44 (1.15)	21.31 (2.14)	2.07 (0.31)	0.065	0.082	10.19	0.25 (0.025)	
R4	rod	9.57 (0.87)	19.87 (1.97)	2.09 (0.29)	0.094	0.103	9.24	0.33 (0.036)	
MP1	multipod pyramid	6.78 (1.21)	11.02 (2.23)	1.65 (0.32)	0.344	0.352	6.54	0.24 (0.037)	3.28 (0.50)
MP2	multipod pyramid	6.98 (0.91)	12.57 (1.44)	1.83 (0.29)	0.342	0.328	6.54	0.44 (0.067)	3.44 (0.53)
TP1	trigonal pyramid	10.21 (0.65)	15.74 (1.90)	1.55 (0.22)	0.104	0.099	8.99	1.22 (0.136)	4.89 (0.54)
M1	multipod	8.31 (0.70)	10.79 (0.93)	1.30 (0.11)	0.311	0.330	6.71	1.60 (0.238)	3.85 (0.57)
TP2	trigonal pyramid	11.87 (0.83)	21.78 (2.79)	1.84 (0.25)	0.084	0.082	9.51	2.36 (0.249)	5.86 (0.62)
M2	multipod	9.38 (1.08)	12.80 (1.72)	1.37 (0.16)	0.261	0.259	7.03	2.35 (0.334)	4.39 (0.62)

[a] The numbers in parentheses for size parameters are standard deviations, assuming a Gaussian distribution. [b] The EFSR rates, k_{s1}^{VHVH} and k_{s1}^{VHHV}, are determined from CPH-3TG signals with VHVH and VHHV polarizations, respectively, with the fitting procedure described in the text. [c] The averages of Δd and $\Delta d/d_{fit}$ for the dots and rods comprising the calibration curve are -0.15 ± 0.36 and -0.021 ± 0.056, respectively.

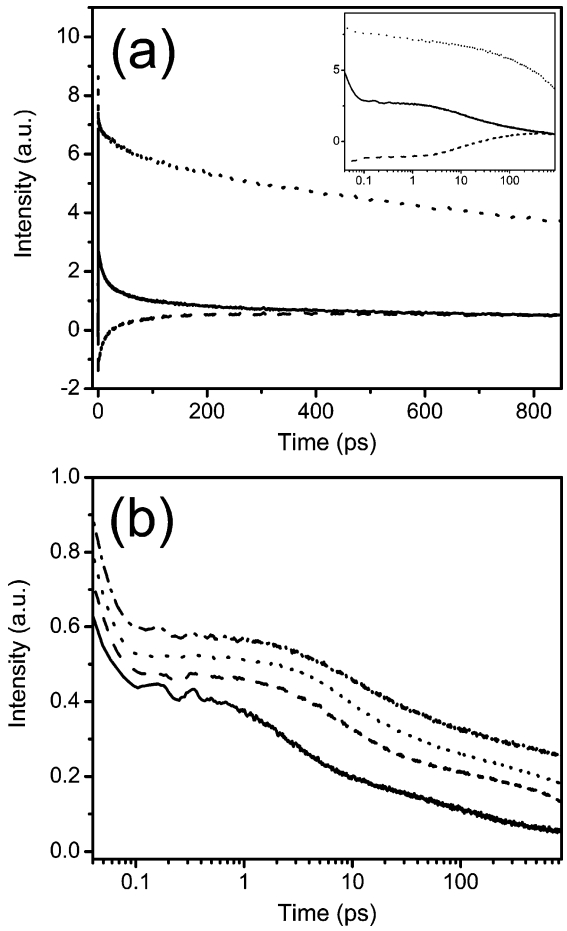

Figure 2. (a) Representative imaginary (absorptive) part of the heterodyned 3-TG data recorded for a NC sample, TP2 (trigonal pyramid). The data for the VHVH (solid), VHHV (dashed), and VVVV (dotted) polarization sequences are shown. Inset: the same 3-TG data plotted with time axis in log scale. (b) The cross-polarized VHVH 3-TG signals for NCs of different sizes and shapes. From bottom to top, each signal corresponds to the samples MP2, B1, R3, and TP2. All the signals are normalized at the maximum intensity, and offsets are added for clarity of presentation.

Here, it should be noted that the EFSR dynamics measured by the CPH-3TG method is not sensitive to the presence of surface states/traps in NCs. For several nanorods reported in our previous studies,[40] we remeasured the 3-TG signals of the aged samples and compared them with the data obtained when the same nanorod sample was fresh. The increase of fast decay components on the several picosecond time scale was manifested in the VVVV signal for the aged sample, showing the increased contribution of surface states/traps to the exciton population relaxation. In contrast, identical decay dynamics were observed in the CPH-3TG signals of fresh and aged samples. Thus, EFSR dynamics is seemingly not affected by the surface states of NCs despite the distinct change in ultrafast exciton population relaxation dynamics.

The EFSR rates, k_{s1}, determined from CPH-3TG measurements are listed in Table 1. Unlike in QDs and nanorods studied in the previous work,[40] it can be seen that the fast EFSR rate of complex-shaped NCs is not directly correlated with the base diameter determined from the TEM images, d_{base}. To perform a systematic analysis on the size and shape dependence of fast EFSR rate, we plotted the EFSR rate with respect to the base diameter, d_{base}, for complex-shaped NCs. We plotted the $1/d^4$ power law fit determined from QDs and nanorods[40,41] together as a calibration curve for the scaling of effective exciton size in the shaped NCs. It can be seen that the data points corresponding to complex-shaped NCs deviate from the $1/d^4$ fit toward larger diameter range with several data points deviating out of the error range of the calibration curve determined from the size distribution of NC samples. In other words, the diameter of base plane overestimates the exciton size in complex-shaped NCs.

To quantitatively measure the degree of deviation for each complex-shaped-NC, we first calculated the diameter (d_{fit}) predicted from the measured EFS relaxation rate using the $1/d^4$ relationship. Then, by subtracting d_{base} from d_{fit}, we defined the deviation of each data point from the $1/d^4$ calibration curve, Δd. In addition, by taking the ratio of Δd to d_{fit}, we normalized the deviation with respect to the size of each NC. These values can serve as quantitative measures

of deviation from the calibration curve for complex-shaped NCs and are listed in Table 1.

Here, it should be noted that the red-edge excitation of the lowest exciton band in our experiments, aimed at exciting only a narrow size distribution of NCs, affects the value of $\Delta d/d_{fit}$ only to a minimal extent. The red-edge excitation selectively excites a subset of larger particles than the ones presented in the TEM images, resulting in the underestimation of either EFSR rate measured by the optical experiments or particle size determined by the TEM measurements. However, the laser center wavelength was tuned to the red from the lowest exciton band by the same amount (5−7 nm) for complex-shaped NCs as for the rods and dots that comprise the calibration curve. Thus, the effect of red-edge excitation is cancelled between the data points of complex-shaped NCs and the calibration curve to the extent whereby the $\Delta d/d_{fit}$ value will be kept at a similar value to when the entire NC size distribution is excited.

From the above analysis, an interesting trend with respect to the shape of NCs can be found: the ratio of $\Delta d/d_{fit}$ increases as the shape deviates from the rod shape and becomes significantly large in trigonal pyramids and multipods. This observation can be explained in terms of increasing structural complexity. For example, in the case of bullet-shaped NCs, the shape is similar to the nanorod except that one end is slightly becoming narrower than in the rod. Therefore, the data points for the bullets are closely overlapped on the power law fit obtained from QDs and nanorods. As the structural complexity increases, however, the effective exciton diameter deviates more significantly from d_{base}. Particularly in multipods and trigonal pyramids, the diameter ratio of the smallest to the largest cross-section in the TEM projection is significantly smaller than that of other shapes of NCs. Accordingly, the effective exciton size in these NCs significantly shrinks compared to the size of the base plane. The extent of deviation for these shapes is quantitatively significant as well, as manifested in the large values of Δd and $\Delta d/d_{fit}$ for multipods and trigonal pyramids. As can be seen in Table 1, the values of Δd ($\Delta d/d_{fit}$) range from 1.22 to 2.35 (0.136 to 0.334) for such shapes of NCs. These values are significantly larger than the average values for dots and rods comprising the calibration curve: $\Delta d = -0.15 \pm 0.36$ and $\Delta d/d_{fit} = -0.021 \pm 0.056$. This result clearly shows the effect of NC shape on the effective exciton size. In other words, the overall shape of NC does matter in determining effective exciton size, although the intricate details of NC shape might not be that important.

To look more closely into the details of how NC shape affects exciton size, we measured the dark-field TEM images of multipod, trigonal pyramids, and multipod pyramids for comparison. (Figure 4) The dark-field TEM image is constructed by collecting electrons scattered off the sample with the central beam and all electrons scattered up to a certain semi-angle blocked by an annular objective aperture in the back focal plane.[43] Thus, in contrast to the conventional bright-field TEM image blurred by artifacts from strong Bragg scattering, a high-resolution and large-contrast ratio image can be obtained in this manner to give an accurate

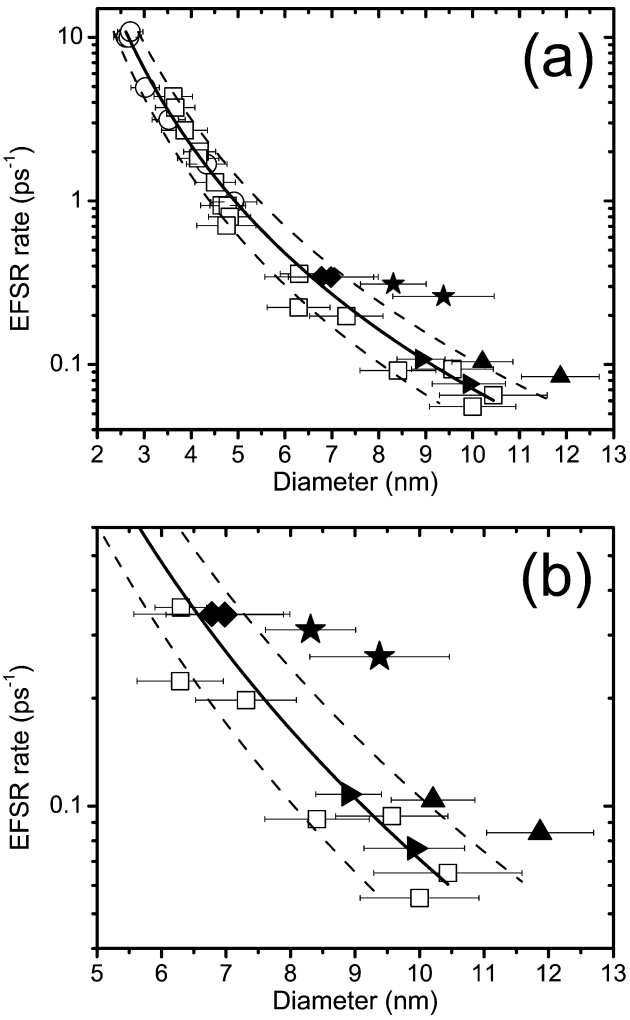

Figure 3. (a) EFSR rates of the complex-shaped NCs plotted versus the diameter of the NC base plane, d_{base}. The data points correspond to bullets (triangles pointing right), trigonal pyramids (triangles pointing up), multipods (stars), and multipod pyramids (diamonds). As a calibration curve, the power law fit of $1/d^{3.8}$ obtained from the data points of CdSe QDs (empty circles) and nanorods (empty squares) is also plotted. The horizontal error bars indicate the standard deviation of the nanocrystal size distribution obtained from TEM analysis, although we believe a much narrower distribution of nanorod sizes was excited in the laser measurement. Two dashed lines below and above the calibration curve represent the error range of the calibration curve arising from the NC size distribution. They were obtained by fitting the data points corresponding to either minimum or maximum diameters of dots and rods in the error range defined by the standard deviations of the NC size distribution. The data points of QDs and nanorods with diameter smaller than 6.3 nm are adapted from refs 45 and 40, respectively. The rods with diameter larger than 6.3 nm (sample R1−R5) are obtained from newly measured CPH-3TG signals in an extended time range. (b) A plot showing the same data as in (a), but the size range where the data points of complex-shaped NCs are mainly located are zoomed in. The large deviation of data points corresponding to multipods and trigonal pyramids are presented distinctively.

3D topology of the imaged objects. In the dark-field TEM image of multipods shown in Figure 4a, the 3D structure of a multipod is clearly identified as either tripod or tetrapod with three or four narrow arms branching out from the center. In Figure 4b, the structure of a trigonal pyramid is character-

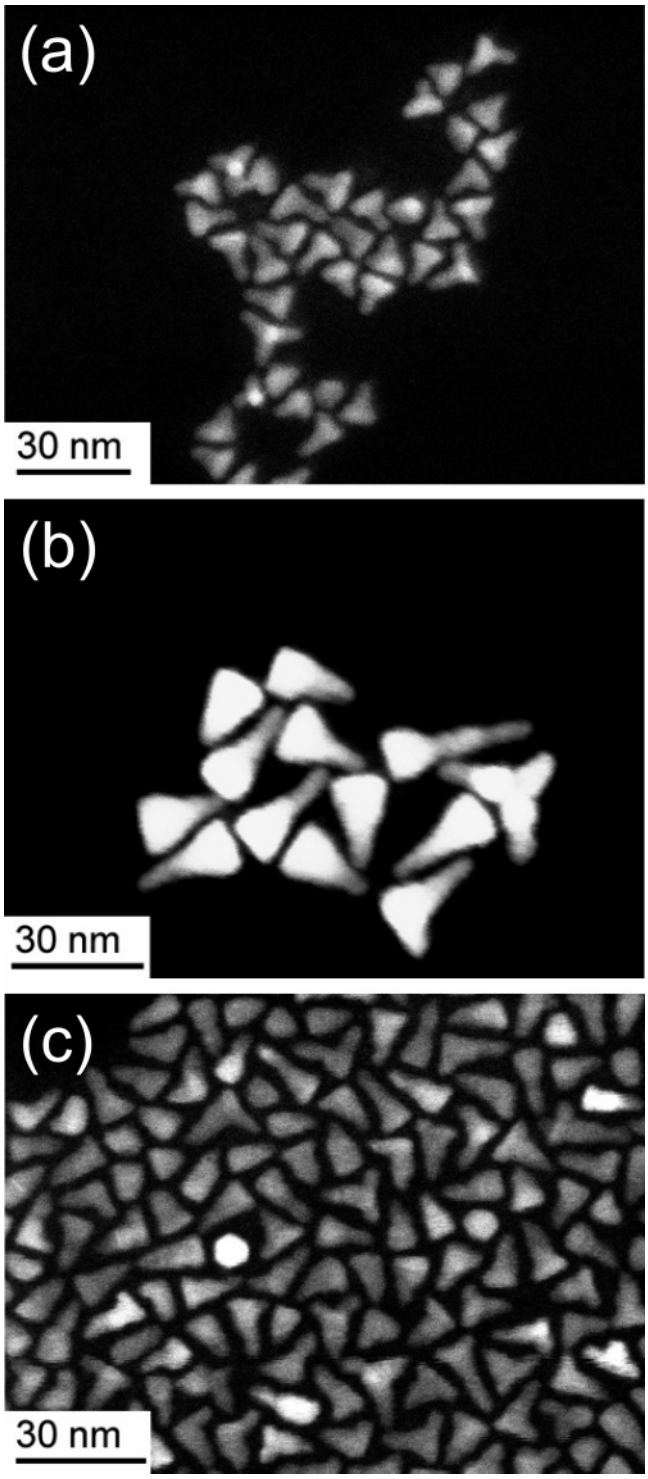

Figure 4. Dark-field TEM images of (a) M1 (multipod), (b) TP2 (trigonal pyramid), and (c) MP1 (multipod pyramid). The 3D topology of the NCs is clearly manifested due to large contrast ratio and lack of Bragg-scattering artifacts. The bright spot represents the local NC structure that bulges toward the viewer. It can be seen that in NCs of a certain orientation an arm of a multipod in (a) or an elongated tip of trigonal and multipod pyramids in (b) and (c) are directed toward the viewer.

ized by a trigonal base plane and a very narrow tip grown perpendicular to the base plane. In contrast, in Figure 4c, a multipod pyramid is identified as a pyramidal shape but having a multigonal base plane with a tip much broader than that of a trigonal pyramid. Also, it has short arms branched from its large base. By comparing the 3D structures of these complex-shaped NCs, the difference in NC volume between them is distinct, explaining the variation in the exciton size (d_{fit}) relative to the overall NC size (d_{base}) depending on NC shape. Narrow and long arms extending from the small center in a multipod and a narrow tip in a trigonal pyramid make the actual confinement volume of an exciton much smaller than the NC size determined from TEM images. In contrast, in multipod pyramids the actual volume inside the NC is significantly large compared to multipods and trigonal pyramids due to the larger area of their base plane and the broader tip. The short arms bulging from the base of a multipod pyramid must have a minor effect on the exciton size. Thus, the NC structures visualized in the TEM images are in agreement with the results of our optical experiments, that is, significantly large $\Delta d/d_{fit}$ values for multipods and trigonal pyramids and small values for multipod pyramids (and bullets).

In addition to the determination of exciton size, we can get a glimpse of the exciton shape when confined in complex-shaped NCs from the above analysis. In (spherical) QDs, the exciton shape is simply spherical owing to the high structural symmetry of the QD. In cylindrical nanorods, the exciton tends to be localized in the center of the rod where the exciton can become elongated over the rod's long axis, resulting in an ellipsoidal exciton shape.[44] Likewise, according to theoretical studies on NCs of pyramidal, teardrop, and arrow shapes, the electronic orbitals, especially the valence band hole orbitals, are locally spread over the large end of NCs rather than its small end.[25,27−29] This theoretical finding can be tested with our results for complex-shaped NCs. To do so, we made the assumption that the exciton in complex-shaped NCs is of spherical shape and then estimated the maximum size of an exciton that could be confined in those NCs. In other words, we calculated the diameter of the largest sphere (d_{sph}) that can fit in a trigonal pyramid whose dimensions were determined by the shape parameters obtained from the TEM images (Table 1). By comparing d_{sph} with the exciton size determined from the calibration curve (d_{fit}) in the analysis described above, we are able to check the validity of the initial assumption of a spherical exciton in the complex-shaped NCs. As can be seen in Table 1, the value of d_{sph} is much smaller than its corresponding value of d_{fit}, being only about half the size. This comparison contradicts our assumption, thus proving that excitons in complex-shaped NCs are not of spherical shape localized in the center of the NCs. Instead, judging from the large estimated exciton size from our analysis, they are likely to be broadly spread over the large end of the NCs, which is in good agreement with the theoretical predictions.

In the present work, we conclude that the shape of a NC affects the size of the exciton confined in the NC, that is, shape matters. Although detailed shape of NCs might not be all that important, the overall shape plays a role in determining the effective exciton size in a NC. Also, the exciton shape was qualitatively determined to be nonspherical, and it is likely that the exciton is predominantly spread

over the large region of complex-shaped NCs such as multipods and trigonal and multipod pyramids, as was predicted by theoretical calculations. We believe that the results of the present work on complex-shaped NCs can inspire further studies to shed more light on the rather subtle implications of NC shape for NC photophysics and their optical properties.

Acknowledgment. The Natural Sciences and Engineering Research Council of Canada is gratefully acknowledged for support of this research. G.D.S. acknowledges the support of an E.W.R. Steacie Memorial Fellowship. The authors thank Neil Coombs and Anna Lee for measuring high-quality TEM images and helpful discussions.

References

(1) Bawendi, M. G.; Steigerwald, M. L.; Brus, L. E. *Annu. Rev. Phys. Chem.* **1990**, *41*, 477.
(2) Norris, D. J.; Efros, A. L.; Rosen, M.; Bawendi, M. G. *Phys. Rev. B* **1996**, *53*, 16347.
(3) Alivisatos, A. P. *Science* **1996**, *271*, 933.
(4) Efros, A. L.; Rosen, M.; Kuno, M.; Nirmal, M.; Norris, D. J.; Bawendi, M. *Phys. Rev. B* **1996**, *54*, 4843.
(5) Gaponenko, S. V. *Optical properties of semiconductor nanocrystals*; Cambridge University Press: Cambridge, 1998.
(6) Bimberg, D.; Grundmann, M.; Ledentsov, N. N. *Quantum Dot Heterostructures*; Wiley: Chichester, 1999.
(7) Klimov, V. I.; Mihkailovsky, A.; Xu, S.; Malko, A.; Hollingsworth, J.; Leatherdale, C.; Bawendi, M. *Science* **2000**, *290*, 314.
(8) Kazes, M.; Lewis, D. Y.; Ebenstein, Y.; Mokari, T.; Banin, U. *Adv. Mater.* **2002**, *14*, 317.
(9) Huynh, W.; Dittmer, J. J.; Alivisatos, A. P. *Science* **2002**, *295*, 2425.
(10) Gur, I.; Fromer, N. A.; Geier, M.; Alivisatos, A. P. *Science* **2005**, *310*, 462.
(11) Yu, P.; Zhu, K.; Norman, A. G.; Ferrere, S.; Frank, A. J.; Nozik, A. J. *J. Phys. Chem. B* **2006**, *110*, 25451.
(12) Klimov, V. I.; Ivanov, S. A.; Nanda, J.; Achermann, M.; Bezel, I.; McGuire, J. A.; Piryatinski, A. *Nature* **2007**, *447*, 441.
(13) Manna, L.; Milliron, D. J.; Meisel, A.; Scher, E. C.; Alivisatos, A. P. *Nat. Mater.* **2003**, *2*, 382.
(14) Lee, S.-M.; Cho, S.-N.; Cheon, J. *Adv. Mater.* **2003**, *15*, 441.
(15) Peng, X. *Adv. Mater.* **2003**, *15*, 459.
(16) Kan, S.; Mokari, T.; Rothenberg, E.; Banin, U. *Nat. Mater.* **2003**, *2*, 155.
(17) Milliron, D. J.; Hughes, S. M.; Cui, Y.; Manna, L.; Li, J.; Wang, L.-W.; Alivisatos, A. P. *Nature* **2004**, *430*, 190.
(18) Yin, Y.; Alivisatos, A. P. *Nature* **2005**, *437*, 664.
(19) Kanaras, A. G.; Sonnichsen, C.; Liu, H. T.; Alivisatos, A. P. *Nano Lett.* **2005**, *5*, 2164.
(20) Cozzoli, P. D.; Pellegrino, T.; Manna, L. *Chem. Soc. Rev.* **2006**, *35*, 1195.
(21) Nair, P. S.; Fritz, K. P.; Scholes, G. D. *Small* **2007**, *3*, 481.
(22) Mohamed, M. B.; Burda, C.; El-Sayed, M. A. *Nano Lett.* **2001**, *1*, 589.
(23) Li, L.-S.; Hu, J.; Yang, W.; Alivisatos, A. P. *Nano Lett.* **2001**, *1*, 349.
(24) Li, X.-Z.; Xia, J.-B. *Phys. Rev. B* **2002**, *66*, 115316.
(25) Li, J.; Wang, L.-W. *Nano Lett.* **2003**, *3*, 1357.
(26) Burda, C.; Chen, X. B.; Narayanan, R.; El-Sayed, M. A. *Chem. Rev.* **2005**, *105*, 1025.
(27) Grundmann, M.; Ledentsov, N. N.; Stier, O.; Bimberg, D.; Ustinov, V. M.; Kop'ev, P. S.; Alferov, Z. I. *Appl. Phys. Lett.* **1996**, *68*, 979.
(28) Stier, O.; Grundmann, M.; Bimberg, D. *Phys. Rev. B* **1999**, *59*, 5688.
(29) Pryor, C. *Phys. Rev. B* **1998**, *57*, 7190.
(30) Tari, D.; De Giorgi, M.; Della Sala, F.; Carbone, L.; Krahne, R.; Manna, L.; Cingolani, R.; Kudera, S.; Parak, W. J. *Appl. Phys. Lett.* **2005**, *87*, 224101.
(31) Banin, U.; Cao, Y.; Katz, D.; Millo, O. *Nature* **1999**, *400*, 542.
(32) Scholes, G. D.; Rumbles, G. *Nat. Mater.* **2006**, *5*, 683.
(33) Salvador, M. R.; Graham, M. W.; Scholes, G. D. *J. Chem. Phys.* **2006**, *125*, 184709.
(34) Kulik, D.; Htoon, H.; Shih, C. K.; Li, Y. *J. Appl. Phys.* **2004**, *95*, 1056.
(35) Le Thomas, N.; Herz, E.; Schops, O.; Woggon, U. *Phys. Rev. Lett.* **2005**, *94*, 016803.
(36) Le Thomas, N.; Allione, M.; Fedutik, Y.; Woggon, U.; Artemyev, M. V.; Ustinovich, E. A. *Appl. Phys. Lett.* **2006**, *89*, 263115.
(37) Wang, J.; Gudiksen, M. S.; Duan, X.; Cui, Y.; Lieber, C. M. *Science* **2001**, *293*, 1455.
(38) Mikkelsen, A.; Skold, N.; Ouattara, L.; Borgstrom, M.; Andersen, J. N.; Samuelson, L.; Seifert, W.; Lundgren, E. *Nat. Mater.* **2004**, *3*, 519.
(39) Scholes, G. D.; Kim, J.; Wong, C. Y. *Phys. Rev. B* **2006**, *73*, 195325.
(40) Kim, J.; Wong, C. Y.; Nair, P. S.; Fritz, K. P.; Kumar, S.; Scholes, G. D. *J. Phys. Chem. B* **2006**, *110*, 25371.
(41) Kim, J.; Wong, C. Y.; Nair, P. S.; Scholes, G. D. University of Toronto, Toronto, Ontario. Unpublished work, 2007.
(42) Scholes, G. D.; Kim, J.; Wong, C. Y.; Huxter, V. M.; Nair, P. S.; Fritz, K. P.; Kumar, S. *Nano Lett.* **2006**, *6*, 1765.
(43) Bals, S.; Kabius, B.; Haider, M.; Radmilovic, V.; Kisielowski, C. *Solid State Commun.* **2004**, *130*, 675.
(44) Shabaev, A.; Efros, A. L. *Nano Lett.* **2004**, *4*, 1821.
(45) Huxter, V. M.; Kovalevskij, V.; Scholes, G. D. *J. Phys. Chem. B* **2005**, *109*, 20060.

NL072149F